PHILOSOPHICAL TRANSACTIONS OF THE ROYAL SOCIETY A MATHEMATICAL, PHYSICAL & ENGINEERING SCIENCES

Temperature Measurement and Melting Determination in the Laser-Heated Diamond-Anvil Cell

Andrew P. Jephcoat and Stanislav P. Besedin

Phil. Trans. R. Soc. Lond. A 1996 **354**, 1333-1360
doi: 10.1098/rsta.1996.0051

Temperature measurement and melting determination in the laser-heated diamond-anvil cell

By Andrew P. Jephcoat and Stanislav P. Besedin

Department of Earth Sciences, University of Oxford, Parks Road, Oxford OX1 3PR, UK

We discuss the problems associated with the measurement of temperature and the determination of melting in the laser-heated diamond-anvil cell. We also briefly summarize the main developments of the last three decades in simultaneous high-P–T measurements and review practical aspects of the technique. The melting curve of argon as a function of pressure has been determined up to 47 GPa, and within experimental error, agrees with a Simon relation extrapolation of the melting curve from previous data to only 1.1 GPa. On the basis of currently debated upper and lower limits for the melting curve of pure iron, the argon melting curve can intersect the melting curve of iron in the range 40–65 GPa. Our experiments suggest that the melting points of iron and argon are equal at 47±1.0 GPa and 2750±200 K. Above this pressure, pure iron would be expected to melt at a lower temperature than solid argon. In a separate experiment, the melting temperature of iron in an argon medium at 57±1 GPa appears greater than 2650±200 K. The intersection of the melting curves for non-interacting materials could serve as standard P–T fixed-points and offer a route to the standardization of different methods of temperature measurement.

1. Introduction

The generation and measurement of simultaneous high pressures and temperatures in the diamond-anvil cell (DAC) has undergone rapid development in recent years. The primary motivation for the generation of such conditions has been the experimental geophysical goal of creation of deep-Earth conditions directly in the laboratory for physical property measurements by spectroscopic, X-ray or other techniques. Such methods are still in their infancy and although generation of high temperatures is readily possible, and sufficient perhaps for initiation of phase transitions, the issue of the measurement and characterization of absolute temperature has become a fundamental problem, especially in relation to melting or the need to understand any derivative thermodynamic property. In particular, a substantial range in the measured temperature of melting (T_m) has been reported for just the principle (end-member) deep-Earth materials: pure iron (Williams *et al.* 1987; Boehler *et al.* 1990; Boehler 1993; Saxena *et al.* 1993; Shen *et al.* 1993; Yoo *et al.* 1993*a*) and silicate perovskite, (Mg,Fe)SiO_3 (Heinz & Jeanloz 1987*a*; Knittle & Jeanloz 1989; Sweeney & Heinz 1993*a*; Zerr & Boehler 1993). That there is a lack of an underlying systematic

Phil. Trans. R. Soc. Lond. A (1996) **354**, 1333–1360
Printed in Great Britain

variation between different experimental groups is becoming clear. The geophysical implications and the possible origins of these differences have been the subject of comments by Brown (1993), Duba (1992, 1994) and are also discussed by Boehler (this volume), Jeanloz & Kavner (this volume) and Lazor & Saxena (this volume).

Although the amount of available data on melting behaviour under pressure is increasing from both DAC and shock-wave studies with an apparently emerging consensus (Chen & Ahrens, this volume; Boehler, this volume; Shen & Lazor 1995), the experimental problems appear sufficiently complex to justify further independent study. The lack of agreement in measured melting temperatures reflects the difficulty in characterization of the state of condensed matter in the DAC at extreme values of pressure and temperature and is intimately connected with the fundamental aspects of temperature measurement. The experimental difficulties can be clearly separated into those related to the observation (identification) of the onset of the melting transition and the measurement (assignment) of an accurate temperature spatially and temporally coincident with the observation.

In the next sections we review the principles of radiometric determination of temperature; aspects of a working laser-heated diamond-anvil cell (LHDAC) system, including calibration procedures, fitting the data and the problem of emissivity. We take the opportunity to summarize the main developments of the last three decades regarding progress in simultaneous high-P–T measurements, make observations on current melting temperatures for selected materials, and finally, present results for the melting of argon and iron and the relative positions of the melting curves. In the work we report in later sections, we have made use of two melting criteria both related to textural change in the sample involving interference contrast under coherent illumination as well as the more direct observation of ablation in thin foils. Jeanloz & Kavner (this volume) and Lazor & Saxena (this volume) survey the advantages and disadvantages of the range of melting criteria used in LHDAC experiments up to the present time.

2. Physical principles and measurement of radiation temperature

The measurement of temperature by radiance methods as opposed to more common methods such as thermocouple thermometry is fundamental in that thermodynamic temperature is explicitly related to the measured radiance: On the latest International Temperature Scale (ITS-90), temperatures above the silver-freezing fixed point at 1234.93 K are now defined through the Planck radiation law (Quinn 1990; Nicholas & White 1994):

$$L_\lambda = \frac{\epsilon(\lambda)c_1}{\lambda^5}\left(\frac{1}{\mathrm{e}^{c_2/\lambda T}-1}\right),$$

where $c_1 = 2\pi hc^2 = 3.741\,774\,9 \times 10^{-16}$ W m^2; $c_2 = hc/k = 0.014\,387\,69$ m K; and $\epsilon(\lambda) = 1.0$ for a blackbody. To transfer the ITS-90 temperature scale above the silver point, c_2 is assigned the value 0.014388 m K (Nicholas & White 1994).

Common radiation thermometric techniques rely on a determination of total radiance from the surface of interest: Light is collected through appropriate imaging optics and the power in a fixed wavelength band falling on a (silicon) detector measured; temperature is then determined through the Stefan–Boltzmann relation (Quinn 1990). Radiance temperature is the temperature of a blackbody with identical spectral radiance to the surface being measured and in this case of spectral-band

radiation thermometry, the surface emissivity is critical to the evaluation of the temperature,

$$\epsilon(\theta, \phi, \lambda, T) = \frac{L_\lambda(\theta, \phi, \lambda, T)|_{\text{source}}}{L_\lambda(\theta, \phi, \lambda, T)|_{\text{blackbody}}}.$$

When directional properties are unimportant, the hemispherical emissivity is (Boyd 1983)

$$\epsilon(\lambda, T) = \frac{M_\lambda(\lambda, T)|_{\text{source}}}{M_\lambda(\lambda, T)|_{\text{blackbody}}}$$

and most closely corresponds to the quantity of interest in the LHDAC. $\epsilon(\lambda, T)$ is the *intrinsic* emissivity of the surface. (We use the term *emissivity* interchangeably with *emittance* to describe any surface, whereas in formal terminology emissivity applies to ideal surfaces only (Quinn 1990).) In the DAC, extrinsic and intrinsic material properties are likely to change with P and T, resulting in an emissivity variation with wavelength which is unknown at the conditions of measurement. The apparent emissivity can depend strongly on surface finish. For example, inconel can show a five-fold variation of emissivity with surface texture and oxidation (Nicholas & White 1994, ch. 8). Prediction of emissivity at high pressure and temperature is therefore difficult or impossible, but one can usually assume a small variation over the visible wavelengths measured in the DAC.

The disappearing-filament optical pyrometer functioned on matching brightness of the sample to a reference filament under the assumption of equal or corrected emissivity. Early pioneering work with the LHDAC by Ming & Bassett (1974) used this method to estimate temperatures. In practical applications of single-wavelength pyrometry (or spectral-band pyrometry now performed with a silicon detector), ϵ is usually estimated independently; for example, in macroscopic applications where the surface of interest may have a known emissivity (Quinn 1990; Nicholas & White 1994). Liu & Bassett (1975) first measured the melting of iron to 20 GPa in the DAC with an internally heated wire, correcting the emissivity to fit the iron melting data of Strong *et al.* (1973) (ϵ was set equal to 0.237 for γ-Fe). In general, an error is introduced if the value of ϵ assumed is incorrect, and for a worst case of $\epsilon = 1$, Heinz & Jeanloz (1987*b*) showed that the difference in measured temperature (brightness) and true temperature can be as much as 50%. Two-wavelength pyrometry makes possible the measurement of temperature from the ratio of spectral radiance, but requires there be negligible wavelength dependence of the emissivity.

In spectroradiometric methods (Jeanloz & Heinz 1984; Heinz & Jeanloz 1987*b*) temperature and an effective (wavelength-dependent) emissivity can be obtained directly from a fit of the Planck function to radiance data over a continuous wavelength range (usually the visible portion of the spectrum for standard detectors). If emissivity is assumed to be less than unity (the greybody approximation) and (nearly) independent of wavelength, or to have the same wavelength dependence as a standard source, then a ratio of radiance data collected over two or more channels (two-colour pyrometry) allows estimation of temperature independently of sample emissivity (Mao *et al.* 1987; Yagi & Susaki 1992).

In the Wien approximation, the irradiance from a greybody is given by the formula:

$$L_\lambda = \frac{\epsilon(\lambda) c_1}{\lambda^5} \left(\frac{1}{e^{c_2/\lambda T}} \right).$$

This approximation is valid to within 4% for temperatures up to 6000 K (Heinz &

Jeanloz 1987*b*). It can be expressed in the form,

$$J_\lambda = \ln \epsilon - \omega T^{-1},$$

where $J_\lambda = \ln[L_\lambda \lambda^5 / c_1]$ and $\omega = c_2/\lambda$. The equation is linear which makes fitting of radiance data more straightforward. We show later a comparison between a direct nonlinear fit of the Planck equation to measured radiance data with the results of the Wien approximation fit, and argue in favour of using the Planck method.

The accuracy of the spectroradiometric method has now been demonstrated by reproducible and concordant results on the melting points of pure metals at or near atmospheric pressure for several independently operating systems (Heinz & Jeanloz 1987*b*; Heinz *et al.* 1991; Saxena *et al.* 1994) as well as through direct comparison with heated thermocouples (Yagi & Susaki 1992). Emissivity is rarely quoted in reports of measured temperatures (except for the estimates made for typical samples by Heinz & Jeanloz 1987*b*), but can in principle offer a diagnostic on the quality of the measurement in the LHDAC (see later section).

3. Experimental systems: description and review

(*a*) *Apparatus*

In this section we describe details of the system we used to make measurements reported in this paper, as well as review general aspects of the method. The techniques are also described in detail by Heinz & Jeanloz (1987*b*), Boehler *et al.* (1990), and Shen *et al.* (1993). Figure 1 illustrates a schematic of apparatus and components. The development of modern one- and two-dimensional silicon diode detector arrays is directly suited to multichannel radiometry and the determination of radiation temperature. This eliminates the need to scan the spectrometer which can impose temporal constraints on stability and effectively provides a parallel system of up to 1024 individual silicon detector channels. The system illustrated includes options for both 1.064 μm (Nd-YAG) and 10.6 μm (CO_2) laser radiation sources and two spectrometer systems – one an imaging system with enhanced astigmatism correction providing spatial resolution along the entrance slit to the spectrometer, the other using a fibre-optic to deliver light to a conventional spectrometer entrance slit. In this paper, we discuss the use of the Nd-YAG (Spectron SL-903) laser radiation source operating either in single-mode, with a polarized, TEM_{00} beam delivering 25 W continuous wave (CW) power (as opposed to pulsed or Q-switched operation), or with an unpolarized, multimode (MM) beam delivering 65 W (CW) power, and combined with a single-core fibre-optic delivery system to either diode-array or CCD detector. Attenuation of the polarized TEM_{00} beam is possible with counter-rotating pairs of quartz plates that impart minimal divergence. In the case of the unpolarized multimode beam, adjustment of the laser pump lamp current can control output power with some sacrifice of laser stability.

The use of TEM_{00} mode makes it possible to focus the beam to *ca.* 10 μm and figure 2 illustrates the quality of focus possible with a TEM_{00} beam on an iron foil in solid argon: adjustment of laser power results in varying spot brightness. We find that the spot diameter can be larger when focused on metal foils than on an insulating surface due to thermal conduction laterally away from the focus (figure 2*c*, *d*). Operation of the laser in multimode with a 50 mm focal-length lens results in broader spot sizes (not less than 0.05 mm) and improved the spectral radiance measurements

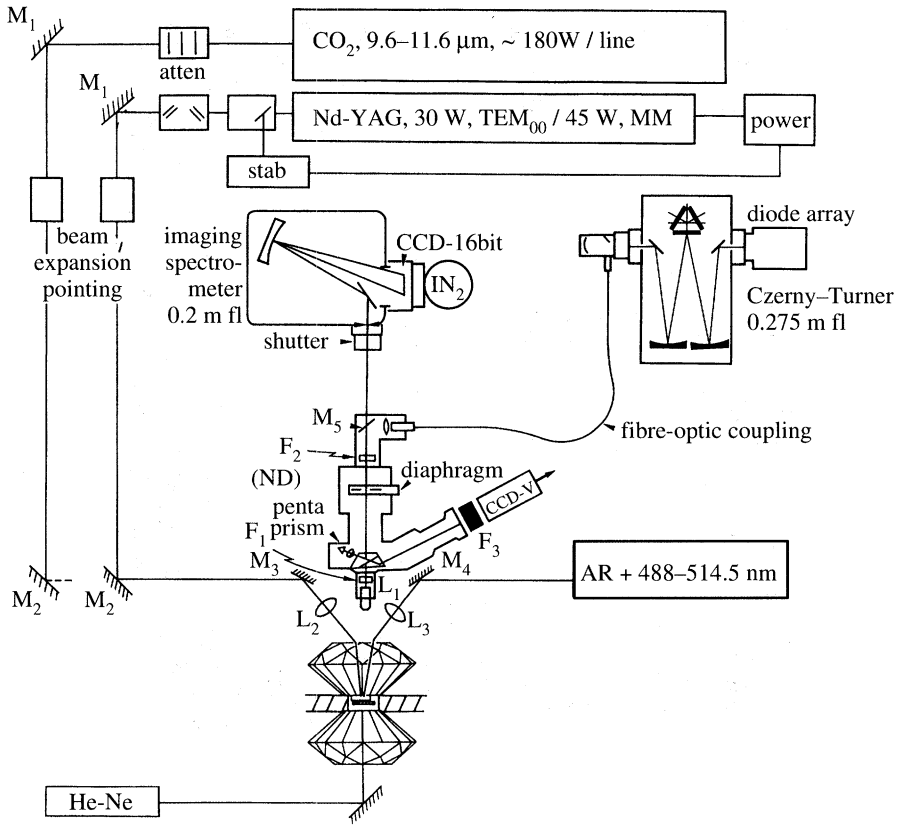

Figure 1. Schematic of a combined CO_2 and Nd-YAG laser-heating system. Imaging spectroscopy is possible with a CCD and imaging spectrometer; alternatively, a fibre-optic connection to a conventional Czerny–Turner spectrometer avoids the need to maintain alignment of the spectrometer slit and the intermediate diphragm (spatial filter) of the optical system. M, mirror; F, filter; L, lens.

which we attribute to uniform temperatures across the spatial filtering aperture. The use of MM beams can in principle solve many of the problems that have been so much discussed in the LHDAC technique especially with regard to the reduction of temperature gradients across the region of the heated spot sampled by the detector. Double-sided YAG laser heating has also been reported to reduce temperature gradients across the heated region (Shen *et al.* 1996) and is essential in X-ray determinations of structural phase transitions. In addition, the use of 45° laser beam delivery geometry through the mirror M_3 in figure 1 is closer to the Brewster angle for diamond (*ca.* 67.5°) and helps to reduce for *p*-polarized beams the loss of incident power due to Fresnel reflection at normal incidence.

The emitted light is collected by either a chromatically corrected, long-working-distance, refracting lens (Leitz-Wetzlar, L25/0.22), L_1, or a reflecting objective (Ealing 15×). A set of neutral-density filters (F_2) can be used to attenuate the intensity of the signal if necessary (Heinz *et al.* 1991). The intermediate, adjustable diaphragm aperture (spatial filter) within the optical system defines the field of view and spatial resolution at the sample. Sampling an *ca.* 3×3 μm area corresponds to an aperture diameter of *ca.* 75 μm with a 25× objective lens. It has been argued that the use

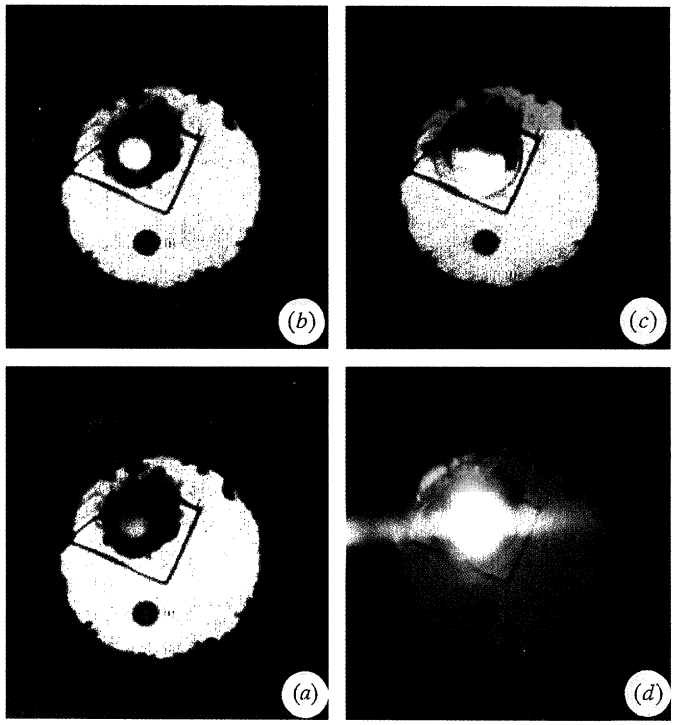

Figure 2. Demonstration of laser-heated spot in the DAC generated with a TEM_{00} mode YAG laser beam focused on iron foil in solid argon at 10 GPa. The foil is resting on a Al_2O_3 wafer to insulate it from the lower diamond within a 0.15 mm hole drilled into a stainless-steel gasket. Transmitted light provides general background illumination through the transparent, solid argon. The panels (*a*)–(*d*) show a progressive increase in intensity of the laser and the axially symmetric focus that can be formed with this mode. Saturation of the video camera used to capture the image takes place in (*d*) as the temperature rises. Temperatures would be measured by collecting light from an area of roughly one fifth the diameter of the hot spot (0.015 mm). A melt boundary between fluid and solid argon is observed in (*c*) and (*d*) as indicated by a dark line roughly following the outline of the heated foil.

of a standard reflecting objective lens may eliminate chromatic errors in the collection of light from the sample (Boehler & Chopelas 1992), but we find that similar results are obtained with each type of lens with the aperturing system used here. Further, reflecting lenses are usually of lower magnification (15×), resulting in reduced spatial resolution and a degraded image quality due to obscuration, both of which are important if textural methods are used to detect melting (see also Jeanloz & Kavner, this volume). In the method described here the intermediate aperture defines the region of the sample from which light is collected for measurement and not the spectrometer entrance slit. A fibre-optic coupling between the spatial filtering aperture and spectrometer is used rather than direct-entrance optics and reduces sensitivity to both position and angular projection of the imaged laser-heated spot at the spectrometer slit, and improves the stability of the alignment. With selected gratings, thermal radiant intensities could be collected over a 460–820 nm range with the CCD detector (Princeton Instruments Inc., lN_2 1152×298 element array) where intensities in the along-slit direction are binned for a single-core fibre optic, or over a range 530–750 nm with a red-enhanced, 700 element, intensified diode-array detector

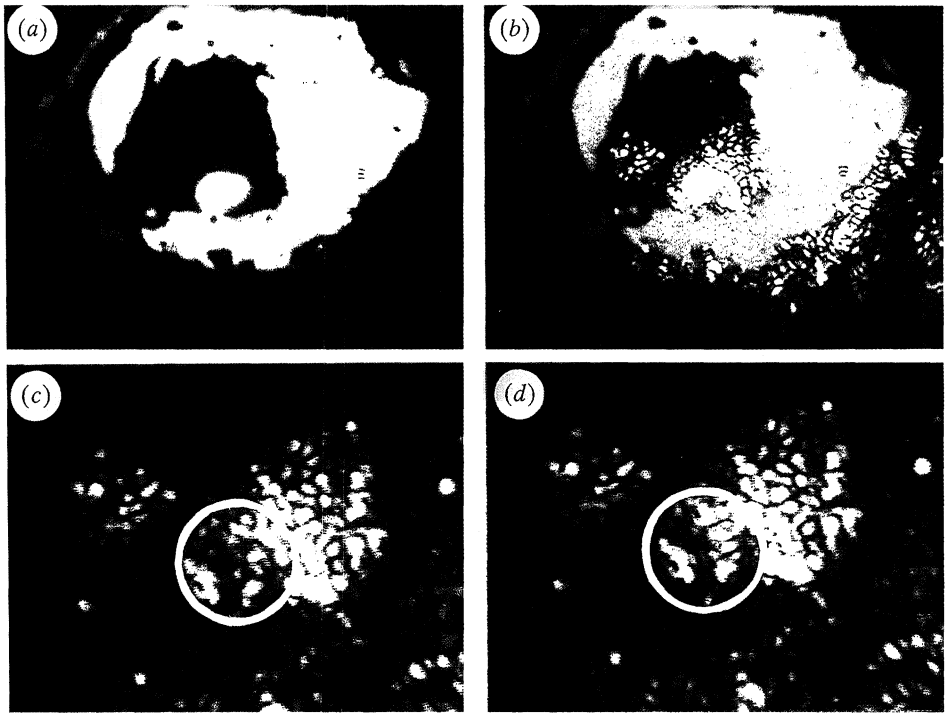

Figure 3. Demonstration of the speckle interference pattern observed through a narrow-pass filter with a sample illuminated with blue 488 nm light of an Ar^+ laser. The size of the hotspot is *ca.* 0.015 mm. (*a*) shows hot spot in transmitted light without laser illumination and filter and (*b*) the speckle pattern generated under coherent light. The circled regions in (*c*) and (*d*) show the slight change in the speckle pattern as observed through the filter and used to determine the melting in solid argon in this study.

(Princeton Instruments Inc., RE/IRY-700). No difference was found between the two detectors operated in this way although the CCD detector provides the advantage of 16-bit dynamic range which can be useful for avoiding saturation with the high light levels encountered. For the studies reported here, we used exposure times of 0.1 s. With the CCD, the electromechanical shutter limits the minimum exposure time to 0.05 s. The diode array can operate continuously with exposure times as short as 0.01 s.

Illumination of the sample during heating is provided by an Ar^+ laser through mirror M_4 in figure 1 operating at 488 nm (Lazor *et al.* 1993) which makes possible visual observation of the sample surface in coherent light through an interference filter, F_3 in figure 1, without obstruction from the (intense) broad thermal emission (figure 3*a*, *b*). A helium-neon laser is used to illuminate the sample from below, through the lower diamond and acts as a marker in sequential exposures: Hole formation in an opaque foil due to melting can be detected from the distinct appearance of the 632.8 nm line in the thermal emission spectrum.

(*b*) *Heating lasers for the DAC and the question of stability*

Active stabilization of the YAG laser is desirable because of characteristic instabilities in the lasing process that transfer to brightness and temperature fluctuations

at the sample. In this case we use a feedback system provided by the manufacturer monitoring the intensity of the output directly and controlling the power supply. Power fluctuations are reduced to 0.1% RMS and similar systems are described by Heinz & Jeanloz (1987*b*) (1–3% RMS), Boehler *et al.* (1990) and Shen *et al.* (1993) (less than 0.5% RMS). Boehler (1992) has since claimed that a YLF laser operating at 1.053 μm provides superior stability of less than 0.1% RMS. Heinz *et al.* (1991) have described a system whereby the sample brightness is used to modulate the incident beam intensity which has the added advantage of smoothing variations due to any temperature-dependent absorption of the sample. Our experience suggests that a stabilized power supply alone is insufficient to remove brightness fluctuations at the sample, and that the system of Heinz *et al.* (1991) is the best option. We did not stabilize the input power on the basis of the sample brightness in these experiments, and for this reason we quote the maximum and minimum temperatures we observed based on sequential acquisitions during heating and melting. Stable laser sources (and by inference sample brightness) have been used to detect solid–solid phase transitions and melting from the laser power – temperature relation (Boehler *et al.* 1990; Saxena *et al.* 1994), a method analogous to conventional calorimetric techniques. The method certainly makes correlation of physical-property change in the sample with temperature possible in a reproducible way and is a strong argument for the use of stabilized systems (Sweeney & Heinz 1993*b*). Further aspects of the power-temperature correlation are discussed by Jeanloz & Kavner (this volume) and Lazor & Saxena (this volume).

Bassett & Weathers (1987) reported use of a pulsed (as opposed to CW) YAG laser system reaching very high peak temperatures with short pulse durations between 200 ns and 50 ms. Temperatures were measured in the same manner as described here except that they used a gated diode-array detector for sequential scans to collect emission spectra during temperature rise and decay cycles. Little work has been done since with pulsed systems. Boehler & Chopelas (1991, 1992) first reported the use of the CO_2 laser with the DAC, though no direct application has been made to studying metals because of problems of high reflectivity and low absorption. Yagi & Susaki (1992) also reported testing CO_2 methods. It seems that radiation near 1 μm (YAG or YLF) is still most suitable for metal melting studies in the DAC. The main advantage of the CO_2 laser is the increased spot size and power, making possible more uniform temperatures when directly absorbed by ceramic (silicate) materials without the need for an inert absorber or the presence transition-metal cations in the (silicate) structure. This advantage has resulted in extensive technical debate in the literature about the benefits of narrow-slit versus wide-slit spectroradiometry as well as various claims on the magnitude of the temperature gradients across the hot spot (see § 2 *e* below).

(*c*) *Calibration of the system response*

In order to obtain temperature and emissivity, measured detector counts, $I(\lambda)$ are transformed (ideally) through the system response function to absolute $L(\lambda)$ which requires use of a source of known spectral radiance. In normal procedures, the system is illuminated with a standard lamp such as a conditioned tungsten-ribbon lamp (Optronics Laboratories Inc. GE550 series (Schneider & Goebel 1984)) calibrated to within 1% against NBS standards and issued with spectral radiance measured as a function of wavelength (see Heinz 1991). Tungsten is the highest temperature filament source available in the laboratory and because melting temperatures can

PHILOSOPHICAL TRANSACTIONS OF THE ROYAL SOCIETY A MATHEMATICAL, PHYSICAL & ENGINEERING SCIENCES

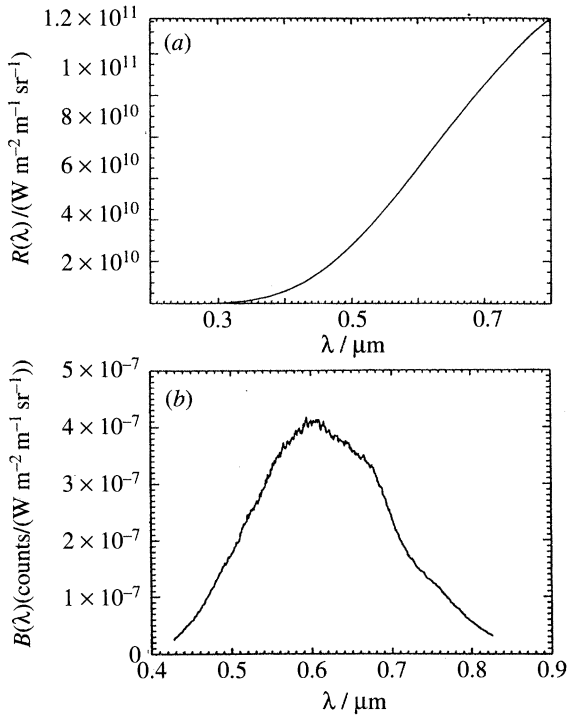

Figure 4. (*a*) Nonlinear fit of the Planck function with emissivity linearly dependent on wavelength: ($\epsilon(\lambda) = \epsilon_{0|\lambda=\lambda_0} + \epsilon_1(\lambda - \lambda_0)$) to the standard radiance data supplied with a tungsten radiance source. T, ϵ_0 and ϵ_1 are free parameters. We obtain $T = 2679.7$ K, $\epsilon_0 = 0.347$, $\epsilon_1 = -0.09\ \mu\mathrm{m}^{-1}$. (*b*) Typical system response, $B(\lambda)$ with refracting lens. This sytem response is the instrument transfer function used to correct measured spectra to absolute $R(\lambda)$ before fitting.

rise rapidly with pressure above laboratory standard sources, the transfer of the calibration to higher temperatures is performed through the Planck law.

A nonlinear, least-squares fit of the Planck function to the radiance data supplied with a calibrated ribbon lamp gives a temperature and emissivity linearly dependent on wavelength that corresponds well to the expected operating temperature of the lamp and the emissivity dependence with wavelength for tungsten. Figure 4*a* shows a fit to the the radiance data supplied with a standard lamp of this kind. Overall system response depends on the absorptive and reflective optical elements, grating efficiency as a function of wavelength, the detector quantum efficiency and responsivity and is shown for the diode-array detector in figure 4*b*. It shows the expected peak in the centre of the visible portion of the spectrum. Measurements of the wavelength dependence of the emissivity of tungsten and other materials are sparse (see Touloukian & DeWitt 1970). Shen *et al.* (1993) used data from Taylor (1952) and Cabannes (1967). A classic determination of the wavelength dependence of the emissivity for tungsten was made by de Vos (1954) showing a decrease over the visible range from about 0.47 to 0.4 at 1600 K. The emissivity also varies with temperature (Nicholas & White 1994, ch. 8).

An important experimental requirement is matching collection of light from the standard radiance source with the geometry of the laser-heated spot in the DAC. In most cases, pinholes are used in order to simulate the size of the laser-heated spot

in the DAC. Transfer of an image of the filament to the pinhole has to satisfy both the aperture conditions used in the original calibration of the standard source and mimic the solid angle of the optics used to collect light from the hotspot in the DAC. We have used a collimator located between the lamp envelope and the long-working distance objective lens focused directly on to the central filament area to match the solid 5° angle of the calibration optics. The Leitz objective lens also contains an internal aperture that can be set to define the aperture of the system.

Tungsten ribbons are calibrated over an area much larger than that of a typical laser-heated spot and may show surface grain-boundary structure (for example, the emissivity from a region between grain boundaries can be higher due to reflection (Quinn 1990)) that could cause problems if imaged at large magnification onto a pinhole even though the lamp has been conditioned. As an aside, we have tested two lamps differing in age by four years with the same stabilized power supply and found negligible difference in system response despite imaging of a *ca.* 3 μm square area of the filament (both lamps were run under the 50 h limit). This fact provides confidence in both stated stability and uniformity of these calibration sources.

Several factors should be considered in evaluation of the system response. In principle, the use of a standard spectral radiance source should provide a system response that is valid no matter what the actual temperature and radiance distribution from the sample are as a function of wavelength, provided the system response is linear. In LHDAC systems, detector linearity is important where intensity varies over several orders of magnitude. For a given exposure time (which is usually short so as to minimize temporal fluctuations) the system calibration from the reference source should remain in the linear region of each diode response. (Linearity of the diodes is generally specified with the array.) The overall system response folds in this intrinsic diode-to-diode response that gives rise to a characteristic shape superimposed on thermal noise across the detector for a given smooth input signal. We tested this directly for different levels of incident illumination. Figure 5*a* indicates that the flatness of each spectrum normalized to a particular incident light level is not strongly dependent on illumination level and so unlikely to contribute to a shift in the apparent level of radiance at different wavelengths that could introduce systematic error into the fitted temperatures.

The system response also includes the effect of diamond through which the hot sample is observed. In practice, it is difficult to include all diamonds intended for use in the calibration optical path before an experiment and is not usually reported. We tested the sensitivity of the response by inserting a diamond anvil in the space between the collimator elements defining the solid angle of the standard lamp filament described above, and found a minimal difference in system response, other than a uniform reduction in overall throughput, as a function of wavelength. Figure 5*b* shows a system response with diamond in the optical path divided by the response without diamond – it should be flat on average within the noise. The diamond appears to transmit uniformly in the visible, although there is some evidence in figure 5*b* of a fall off at high pixel number (long wavelength) which suggests that the red portion of the response could be modified by diamond. Transmission through the diamond is dominated by Fresnel reflection losses at the diamond surface and may in cases where sample refractive index changes with pressure (for example if a rare-gas solid is included in the chamber) be impossible to calibrate out directly, making it difficult to obtain an absolute emissivity of the sample. Other variable effects may arise from fluorescence of diamond due to probe beams or the thermal emission of the sample.

PHILOSOPHICAL TRANSACTIONS OF THE ROYAL SOCIETY A MATHEMATICAL, PHYSICAL & ENGINEERING SCIENCES

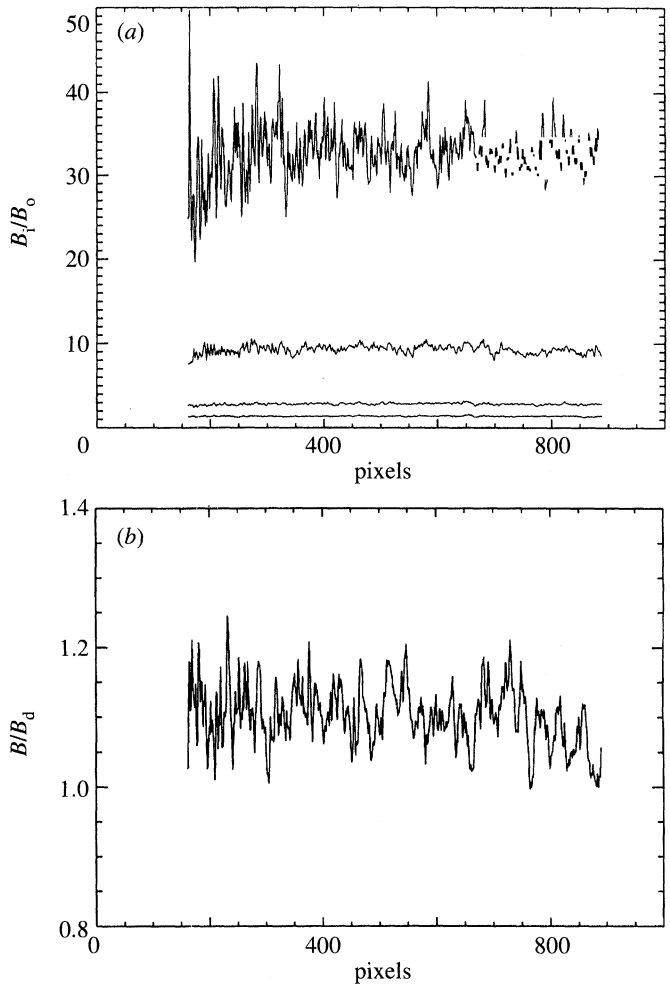

Figure 5. (*a*) Tests of system linearity (B_i/B_0) for different proportions of count saturation of a 14-bit linear diode array; (*b*) Measured system response with and without diamond, B/B_d. Tests for several type I diamonds indicate that there is a small effect on spectral shape, with slight reduction of red response and a uniformly reduced transmitted intensity.

(*d*) *Fitting temperature and emissivity*

In the determination of temperature, wavelength-dependent effects dominate the accuracy rather than changes that effect the throughput of the system uniformly. If the system throughput is attenuated across all wavelengths compared to the transmission used to obtain the system response calibration, then the emissivity obtained from a fit is altered by a constant scale factor to match the measured effective spectral radiance. We find with a TEM_{00} beam that small drift in focus or underfilling of the aperture can change the effective emissivity of a sample. Depending on the magnitude of the difference in system transmission, the emissivity may take on non-physical values. For this reason, fixing the emissivity dependence on wavelength *a priori*, modifies temperature estimates (Lazor *et al.* 1993; Heinz *et al.* 1991), but there is no firm basis for expecting this dependence to be valid for a given system calibration, or in the DAC because emissivity depends on additional extrinsic properties.

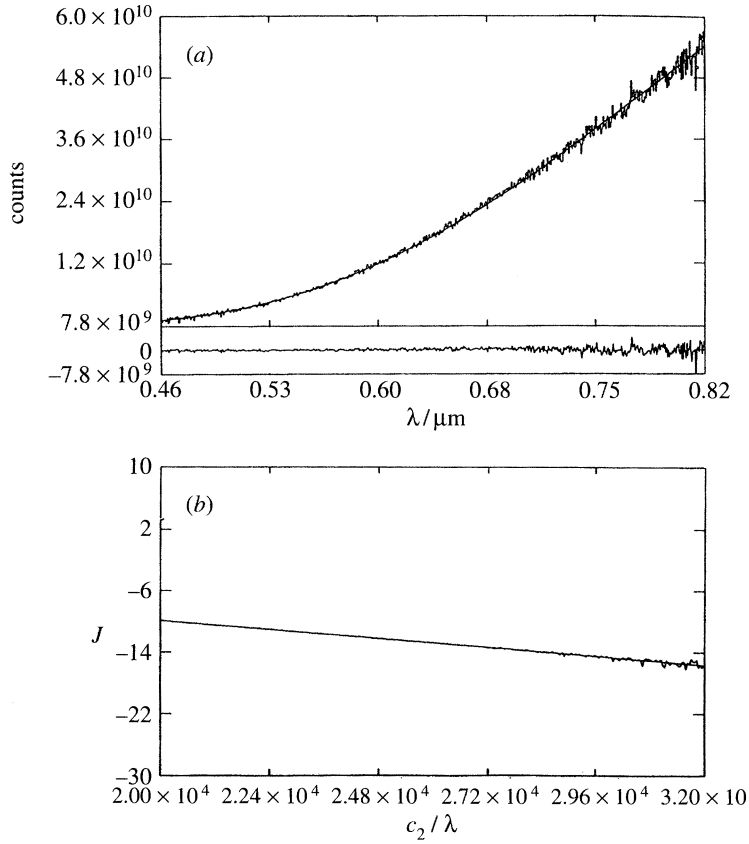

Figure 6. (*a*) Example fits of the Planck function to emission spectra, corrected for system response, from a platinum foil surface heated to melting with 1.064 μm radiation. Fitted temperatures in the range 1997–2070 K, agree well with the published melting temperature, $T_m = 2065$ K. (*b*) Fit produced to same data using the linear, Wien approximation with constant emissivity (greybody). J and c_2 are defined in § 2.

Confirmation of the accuracy of the system is shown in figure 6 with an example of a spectrum obtained from platinum foil at 1 bar. Both Planck and Wien fits to the corrected radiance data with the system response of figure 4*b* are shown. The melting temperature agrees well with published values and emissivity decreases with wavelength over the visible.

Although emissivity can be obtained as an explicit function of wavelength when fitting multichannel data, its absolute value depends critically on the geometry of the calibration lamp matching the emission geometry of the laser-heated hot spot. If there is a difference in emission geometry (for example the laser-heated spot does not fill the spatial aperture) then the effective emissivity measured will differ from the absolute value, but will not affect the measured temperature. If the apparent emissivity changes non-physically (for example due to temperature fluctuations, or temperature gradients are sampled) then it is likely that the measured radiance data will not fit well to the Planck equation for any emissivity variation allowed in the fit. Figure 7*a* shows a corrected set of radiance data that did not fit well to the Planck function and figure 7*b* shows the same data processed with the Wien approximation which appears insensitive to the quality of fit. In the nonlinear fitting procedure,

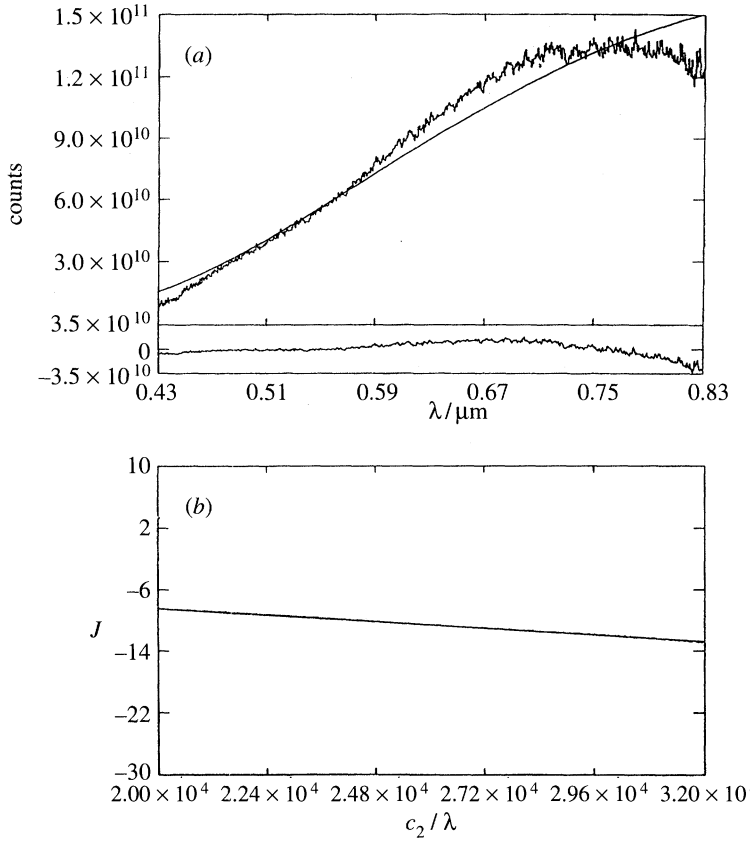

Figure 7. An example of response-corrected thermal emission data from the LHDAC. (*a*) Fitting of the Planck equation (even with a variable linear emissivity term) is poor as shown in the difference panel. The data were obtained from an iron foil sample in a solid argon medium at 50 GPa with a focused TEM_{00} beam. The data cannot be well fitted for reasonable values of temperature and emissivity. The problem becomes less frequent with the use of multimode beams implying that temporal and spatial instability of the hot spot under the aperture bias the radiance as a function of wavelength. (*b*) The same data processed in the linear Wien approximation with constant emissivity. This procedure is much less sensitive to the deviation of the data from a proper Planck form.

it is not practical to use more than two adjustable parameters for the emissivity dependence on wavelength over the range of the experiment (figure 7*a*). Fits to spectral radiance data occasionally also result in unexpected or non-physical behaviour of the emissivity (for example, a rapid change of emissivity with wavelength over 400–800 nm) and can be used to gauge the reliability of the measurement.

Finally, we note that Gillet *et al.* (1993) describe a method which claims to bypass the need for an analytical fit of the Planck equation by computer-matching the spectral shape of the measured thermal emission with distributions of thermal intensity previously determined at known temperature.

(*e*) *Sampling of light from the hot spot*

Measurement of temperature in the LHDAC by necessity requires a choice of sampling method for the small emission region and delivery of light from this region to the spectrometer. Two distinct methods – 'narrow-slit' and 'wide-slit' have been

described in the literature leading to extended debate on the advantages of each (Heinz *et al.* 1994; Boehler & Zerr 1994; Boehler, this volume; Jeanloz & Kavner, this volume; Lazor & Saxena, this volume). In the narrow-slit method, the spectrometer entrance slit, or an intermediate aperture, is used to spatially filter the image of the hot region. Wide-slit methods involve collection of all the light from the heated area and scanning a perpendicularly oriented sampling slit along the spectrometer entrance slit. Transform methods have then to be used to reduce the data and are described in detail by Jeanloz & Heinz (1984), Heinz & Jeanloz (1987*b*), Williams *et al.* (1991), and Jeanloz & Kavner (this volume). Given the difficulty of the experiments and maintaining temporal stability, it is impressive that this method can be applied. The method we have described here falls into the narrow-slit category, except that we are not using the spectrometer entrance slit directly as the spatially resolving aperture, but an intermediate aperture as described above. Furthermore, we underfill the connecting fibre with a refractive lens and we use reflecting optics to match the numerical aperture of the spectrometer which largely avoid the problems reported by Jeanloz & Kavner (this volume) on diffraction effects from apertures. In a static optical system, any effects of diffraction by the optical elements should be accounted for in the system response calibration. It is also unnecessary with this system to use an optic for correcting for the dispersion of diamond and the chromatic aberrations to image quality (Boehler & Chopelas 1992). We do assume that we can sample a discrete and small enough region of the laser-heated spot to obtain a point measurement of the temperature profile without taking explicit account of temperature gradient corrections. This assumption seems well justified with multimode heating. Furthermore, by measuring from a heated foil we are taking light from a hot surface rather than a finite volume of sample. Other heating geometries and temperature corrections in dielectric samples are discussed by Bodea & Jeanloz (1989).

As discussed out by Jeanloz & Kavner (this volume), the use of an imaging detector can potentially remove the need for all spatial filtering. This technique requires a spectrometer with corrected optics (usually an aberration-corrected holographic grating) to transfer faithfully the image at the spectrometer entrance slit to the exit slit and detector. Despite the corrections claimed in commercial instruments, such systems from our experience may not offer sufficient spatial resolution along the slit to provide independent slices of the temperature distribution unless the image of the spot is further magnified to a size of the order of the entrance slit length.

4. A brief summary of melting observed at high pressures

(*a*) *Iron*

Shock-wave techniques provided the first experimental means to study materials at simultaneously extreme pressure and temperature. Al'tshuler *et al.* (1962) and McQueen *et al.* (1970) presented the first temperatures calculated along the Hugoniot of iron (the locus of associated shock and particle velocities). The methods developed extensively into the 1980s with new measurements of sound wave velocity (release wave velocities) along the Hugoniot for iron. These velocity measurements were sufficiently sensitive to detect phase transitions and melting along the Hugoniot (Brown & McQueen 1980, 1982). Hugoniot temperatures had to be calculated (McQueen *et al.* 1970) and culminated in two fixed P–T points in the phase dia-

PHILOSOPHICAL TRANSACTIONS OF THE ROYAL SOCIETY A MATHEMATICAL, PHYSICAL & ENGINEERING SCIENCES

gram of iron: a transition at 200±2 GPa and 4400±300 K associated with the ϵ–γ transition and at 243±10 GPa and 5500–6000 K, associated with the melting point of γ iron. Refinements in the calculated temperatures, depending on estimates of the electronic contributions to specific heat and value of the Grüneisen parameter, resulted in slight adjustments to the melting temperature at 243 GPa to 5000–5700 K (Brown & McQueen 1986).

Direct methods to measure temperature in shock-wave experiments used the measured radiance from the surface of a sample deposited on transparent anvil substrates as part of the target assembly. Temperature is determined by identical methods to the LHDAC from the radiance measured through the anvil in the greybody approximation (Kormer *et al.* 1965; Schmitt & Ahrens 1984; Bass *et al.* 1987 and references therein; Svendsen *et al.* 1989). An important aspect of these measurements on iron is that the temperature obtained at the sample-anvil surface has to be corrected for anvil thermal conductivity and the sample-anvil impedance mismatch (Bass *et al.* 1987) and requires knowledge of transport properties at extreme pressure and temperature, none of which had been measured at the time. The measurements on iron produced high Hugoniot temperatures (for example, 6700±400 K at 243 GPa) that were consistent with the initial calculated temperatures of McQueen *et al.* (1970), but significantly higher than the revised figures of Brown & McQueen (1986). Further, the temperature data quoted were selected from an overall set of data with significantly higher measured temperatures that were attributed to problems in sample preparation. Melting is not determined directly in these experiments and in fact should show as a discontinuity in the P–T path along the Hugoniot (Kormer 1968). The discontinuity observed by Bass *et al.* (1987) was small, and not strongly constrained by all the data. Nellis & Yoo (1990) reviewed the problems associated with measuring temperature in shock-wave experiments.

The first DAC heating measurements on iron wires were made by Liu & Basset (1975) to 20 GPa, but temperatures were dependent on the emissivity assumed and fitted to earlier data: the melting of iron was already well known up to the γ–δ–l triple point and along a 0.5 GPa section of the γ-liquid transition to 5.7 GPa (less well calibrated work in the 1960s was superseded by Strong *et al.* (1973)). Boehler (1986) obtained data on the slope of the γ–ϵ transition line of iron and the melting slope of the γ phase with a wire-heating technique to 43 GPa. The γ–ϵ slope, 28.6 K GPa^{-1} obtained differed from that obtained by a similar technique of Mao *et al.* (1987) to 36 GPa (35 K GPa^{-1}). Williams *et al.* (1991) argued that the larger wire (20 μm) used in the Boehler (1986) experiment led to lower temperature estimates due to uncorrected temperature gradients when compared to the 10 μm wire of Mao *et al.* (1987).

Static DAC melting data on iron to in excess of 100 GPa were first reported by Williams *et al.* (1987). in which bracketed observations of 'melt' and 'no-melt' were used to define the trajectory of the melting curve. A description of the inversion technique and correction for peak versus average measured temperatures for the DAC experiment was presented by Williams *et al.* (1991) to support their observations. These data were in agreement with the melting slope of Liu & Bassett (1975), but in disagreement with the data (wire in Al_2O_3) of Boehler (1986) leading to the question of proper correction for temperature gradients (Williams *et al.* 1991). A combination of the DAC data to 100 GPa with the shock-measured temperature data obtained at that time (Bass *et al.* 1987) resulted in an empirical melting curve of iron being drawn smoothly through the static data to coincide with the apparent discontinuity

PHILOSOPHICAL TRANSACTIONS OF THE ROYAL SOCIETY A MATHEMATICAL, PHYSICAL & ENGINEERING SCIENCES

Table 1. *Brief history of the major developments in high-P–T studies on iron*

reference	method	comment
Al'tshuler *et al.* 1968	SW	calculated Hugoniot temperatures
McQueen *et al.* 1970	SW	calculated Hugoniot temperatures
Liu & Bassett 1974	DAC	$P \approx 20$ GPa, heated wire
Brown & McQueen 1980	SW	sound-velocity discontinuity
Brown & McQueen 1986	SW	sound-velocity discontinuity: 200, 243 GPa
		$T_m \approx 5000$–5700 K at 243 GPa
Boehler *et al.* 1986	DAC	$P \approx 43$ GPa, ϵ–γ, heated wire
Williams *et al.* 1987	DAC	$P \approx 100$ GPa, $T_m \approx 4000 \pm 400$ K
Bass *et al.* 1987	SW	$P \approx 243$ GPa, $T_m \approx 6700 \pm 400$ K
Boehler *et al.* 1990	DAC	$P \approx 120$ GPa, $T_m \approx 3000$ K
Boehler 1993	DAC	$P \approx 200$ GPa, $T_m \approx 3750$ K
Saxena *et al.* 1993	DAC	$P \approx 50$ GPa, $T_m \approx 2700$ K (max), β-Fe reported
Yoo *et al.* 1993*a*	SW	$P \approx 235$ GPa, $T_m \approx 6350$ K
Saxena *et al.* 1994	DAC	$P \approx 150$ GPa, $T_m \approx 3500$ K (max)
Saxena *et al.* 1995	DAC	X-ray β-phase structure: *dhcp*
		40–60 GPa, MgO pressure medium
Yoo *et al.* 1995	DAC	X-ray stability of ϵ phase, $P \approx 50$–110 GPa,
		$T \leqslant 3500$ K, Al_2O_3 pressure medium
		γ–ϵ–l point at 2500 ± 200 K and 50 ± 10 GPa

attributed to melting along the Hugoniot (Williams *et al.* 1991). In this sense the two sets of data were mutually consistent.

Subsequent LHDAC work led to an increased pressure limit over which the melting point of iron was determined, first in argon to 35 GPa, continued in Al_2O_3 to 120 GPa (Boehler *et al.* 1990) and later extended to 200 GPa also in an Al_2O_3 medium (Boehler 1993). Melting temperatures obtained in this DAC work were significantly lower than the shock data with evidence for a triple point near 100 GPa. Furthermore, reconciliation of the two techniques required invoking the existence of new phases for which there is scattered evidence (Boehler 1993; Saxena 1993; Boehler, this volume). The existence of these phases can be addressed through direct determination of the the phase diagram of iron and has been attempted through simultaneous synchrotron X-ray diffraction experiments in the LHDAC: Yoo *et al.* (1995) report that ϵ-iron is stable from 50 to 110 GPa at high temperature which contradicts the conclusion that the new (β) phase reported by Saxena *et al.* (1993, 1995) is a structural change. The ϵ–γ–l triple point is lowered to 50 ± 10 GPa and 2500 ± 200 K. Above 110 GPa, there is little constraint on the stable phase of iron. Such experiments also offer the possibility of using an X-ray criterion for melting, but will depend critically on alignment and the exclusion of low-temperature solid from the X-ray scattering volume. Table 1 summarizes the major shock-wave and DAC melting and structural experiments on iron.

Independent measurements of iron shock temperatures by Yoo *et al.* (1993*a*) obtained Hugoniot temperatures in agreement with those measured previously below

Table 2. *Summary of melting studies of* $(Mg, Fe)SiO_3$

reference	method	comment
Heinz & Jeanloz 1987*a*	DAC	$P \approx 20$–65 GPa, $T_m \approx 3000 \pm 300$ K
Knittle & Jeanloz 1989	DAC	$P \approx 96$ GPa, $T_m \approx 3800 \pm 300$ K
Sweeney & Heinz 1993	DAC	$P \approx 80$ GPa, $T_m > 2500$ K
Zerr & Boehler 1993	DAC	$P \approx 62.56$ GPa, $T_m \approx 5000 \pm 200$ K

250 GPa. Iron melting occurred in these studies along the Hugoniot at 235 GPa and 6350 K (Yoo *et al.* 1993*a*). The expected break between solid and liquid Hugoniots was clearly resolved in these experiments and consistent with the transition identified by Brown & McQueen (1986); these measurements were also dependent on a thermal model of the iron-substrate interface (in this case, diamond which gave a better impedance match). These new data failed to resolve the discrepancy between the LHDAC and shock-wave temperature estimates. Various arguments have been made (see this volume) for the apparent lack of agreement, but no convincing explanation appears accepted at this time, unless there is a systematic error in shock temperature estimates based on errors in the values of transport properties at high pressure and temperature. The implications for core temperatures are discussed by Duba (1992) and Jeanloz & Kavner (this volume).

Birch (1972) provided the first discussion of the risks involved in working with low-pressure melting data when making inferences on core properties and a framework for the debate on the position of the γ–ϵ–l triple point. At the present time, Anderson (1990, 1995) and Anderson & Duba (1996) provide the most exhaustive review of the implications of contemporary experiments on iron for the triple-point problem and the (unknown) phase diagram of iron at core conditions. Ironically, following the extensive recent debate over the current melting experiments, the cautious application by Simon (1953) of the Simon–Glatzel (SG) relation to iron resulted in a prediction of the range of melting temperatures expected at core pressures that agrees within error with the data of Boehler (1993) to 150 GPa. This agreement for iron is probably fortuitous, taking no account of transitions in the solid phase; the failure of the SG law and other empirical melting laws to predict melting in materials other than simple molecular solids is well documented (see, for example, Kennedy & Vaidya 1970; Ross 1969; Stixrude & Bukowinski 1990).

Despite the possibility of a new phases resolving the mismatch in iron melting, debate on this problem would most immediately benefit from further agreement on the melting temperature of iron determined by separate methods.

(*b*) *Iron–magnesium silicate perovskite*

In parallel with the iron melting efforts, several reports on the melting of perovskite were made that appeared similarly in poor agreement. These are included here briefly for completeness and summarized in table 2. The original measurements by Heinz & Jeanloz (1987*a*) on $Mg_{0.9}Fe_{0.1}SiO_3$ produced a flat melting curve in the range 23–60 GPa. In these experiments temperature gradients were taken into account in obtaining final temperature estimates. Knittle & Jeanloz (1989) continued the work to 96 GPa finding a change to a positive slope of 19.5($\pm$5.5) K GPa^{-1}

above 60 GPa, with estimated melting of 3800(±300) K at 96 GPa. Sweeney & Heinz (1993*a*) obtained lower temperatures, that were reported to be unrepresentative of the true melting temperature (Heinz *et al.* 1994), but they did not find evidence of a change in slope. Zerr & Boehler (1993) measured the melting of two compositions of perovskite (natural $Mg_{0.88}Fe_{0.12}SiO_3$ and synthetic $MgSiO_3$) in an argon medium obtaining 5000±200 K at 62.5 GPa, independent of composition and significantly higher than the earlier work. The origin of the discrepancy between these results has led to detailed analysis on the best way to make measurements in the LHDAC (Brown 1993; Heinz *et al.* 1994; Boehler & Zerr 1994; Boehler, this volume; Jeanloz & Kavner, this volume; Lazor & Saxena, this volume) with the key difference resting on the hot-spot sampling technique and the accounting of temperature gradients. The results suggest that a systematic difference is not responsible for the difference in the measured iron melting temperatures. Early theoretical predictions of the perovskite melt curve were varied and offered little guidance on the likely melting temperatures (Ohtani 1993; Poirier 1989; Stixrude & Bukowinski 1990). The data of Zerr & Boehler agree most closely with the simulation of Ohtani (1993) and the melting slope is compatible with multianvil measurements below 25 GPa. Belonoshko (1994) claim agreement with the high-temperature melting data in a two-phase MD simulation.

(*c*) *Iron compounds, oxides and metals*

The expected alloying of iron in the outer core of the Earth (Poirier 1994) has led to a number of studies on binary iron compounds. A principle concern is the effect of light component on melting point depression and core temperatures (Williams *et al.* 1990; Boehler, this volume; Boehler 1996). Here we briefly examine some of this data, subject to the same problems of temperature measurement and melting onset determination, from the point of view of any consistency in LHDAC techniques. For wüstite, Shen *et al.* (1993) agree closely with the data of Boehler (1992), where an argon medium was again used, above 25 GPa, but below this pressure their melting data fall roughly between these and the higher melting temperature data obtained by Knittle & Jeanloz (1991) (*ca.* 700 K higher at 50 GPa). Duba (1992) again comments on these differences, the implication being that core-mantle boundary temperatures are lower than previously thought. Chemical effects, oxidation state and sample purity are likely to affect the solid–melt transition in the case of $Fe_{1-x}O$ masking systematic differences. For FeS (troilite), the melting temperatures obtained by Williams & Jeanloz (1990) using tomographic inversion and Al_2O_3 media are again *ca.* 500 K higher than the Boehler (1993) determination in an argon medium. If one compares data for different materials as a whole, however, the melting temperatures of iron (Boehler 1992; Shen *et al.* 1993), wüstite (Boehler 1992; Shen *et al.* 1993), and FeS (Boehler 1993), for example, would not be significantly different within a few hundred kelvin error bar at 50 GPa.

Zerr & Boehler (1994) have recently reported the melting curve of MgO to a maximum melting temperature near 4000 K at 32 GPa. The initial slope is a factor of three lower than first-principles models of both Cohen & Weitz (1997) and Vočadlo & Price (1996). The disagreement here is also difficult to reconcile (experiment *ca.* 1500 K lower at 30 GPa) because changes in the calculated melting temperature would require 'exotic' properties of MgO liquid (Cohen & Weitz 1996).

In other LHDAC experiments on metals, the melting of nickel has been determined to 70 GPa (Lazor *et al.* 1993) where T_m at 50 GPa is 2500 K (almost identical to the

PHILOSOPHICAL TRANSACTIONS OF THE ROYAL SOCIETY A MATHEMATICAL, PHYSICAL & ENGINEERING SCIENCES

melting temperature reported for iron (Shen *et al.* 1993)) and uranium melting has been determined to 40 GPa (Yoo *et al.* 1993*b*).

(*d*) *Argon*

A major motivation for study of melting of the rare-gas solids (RGS) and other simple-molecular solids characterized by weak, long-range attractive forces and strong, short-range repulsive forces, was that these materials were more readily treated theoretically and make possible tests of melting theories to high compressions (see, for example, Stishov 1975; Loubeyre 1989). The SG equation has been frequently used to parametrize the melting curves in either of two forms,

$$P = A[(T/T_0)^c - 1] + P_0$$

and

$$P = AT^c + B,$$

where P and T are the pressure and temperature at melting, P_0 and T_0 are the corresponding triple point values, and A, B, and c are fitted parameters (Hardy *et al.* 1971). Early work on the melting of argon and recent theoretical predictions are summarized in table 3. Hardy *et al.* (1971) obtained precise measurements in a pressure vessel for argon melting to 1.1 GPa with the following parameters:

$$P_{\mathrm{Ar}}\,(\mathrm{bar}) = 2.673T(\mathrm{K})^{1.523} - 2293.35.$$

The highest pressure melting data reported recently for argon are to 6 GPa and 717 K (Zha *et al.* 1986) determined from grain boundary disappearance up to 3.6 GPa and discontinuous shifts in the interference pattern above this pressure. These data are consistent within error with the parameters of Hardy *et al.* (1971).

Ross (1969) showed that the SG relation followed from a generalized Lindemann melting law that could be reduced to a relation of the form:

$$P_{\mathrm{m}} = P(0, v_{\mathrm{m}}) + a(T_{\mathrm{m}}/T_0)^d.$$

The term $P(0, v_{\mathrm{m}})$ is the pressure at 0 K and volume v_{m}, with a and d constants that are related to the exponent, n, of the inverse power form used to describe the pairwise, additive repulsive forces in dense argon (Ross 1969). If $P(0, v_{\mathrm{m}})$ is constant, then the above relation has the SG form. Variation of $P(0, v_{\mathrm{m}})$ with pressure, therefore, is expected to result in the breakdown of the SG relation at high compressions. Theoretical calculations of the melting curve for argon have been presented by Ross (1973) to 12.8 GPa and in Zha *et al.* (1986) to 53.2 GPa from an intersection of Gibbs free energy isotherms obtained form separate models of the liquid and solid. Belonoshko (1992) has calculated the melting curve to over 3500 K with a molecular dynamics method. Results of these theoretical techniques appear largely consistent. In the next section we present results on the melting of argon to 47 GPa.

5. The relative position of the iron and argon melting curves

The use of RGS in DAC experiments is now common in order to provide a transparent, inert medium and reduced pressure gradients. In laser heating studies, the low thermal conductivity of these materials is also essential for insulating a heated sample from the diamond surfaces. One advantage of RGS is the effective displacement of oxygen trapped in grain boundaries during loading of solid media. In our

PHILOSOPHICAL TRANSACTIONS OF THE ROYAL SOCIETY A MATHEMATICAL, PHYSICAL & ENGINEERING SCIENCES

Table 3. *Selected argon melting studies*

reference	method	comment
Experiment		
Simon *et al.* 1930		$P \approx 0.51$ GPa
Bridgman 1934		$P \approx 0.59$ GPa
Robinson 1954	magnetic pellet	$P \approx 0.84$ GPa
Michels & Prins 1962	blocked capillary	$P \approx 0.15$ GPa
Lahr & Eversole 1962	piston-cylinder	$P \approx 1.8$ GPa
Grace & Kennedy 1967	piston-cylinder	$P \approx 2.6$ GPa
Crawford & Daniels 1968	pressure vessel	$P \approx 0.634$ GPa, 201.32 K
Stishov *et al.* 1970	pressure vessel	$P \approx 1.58$ GPa
Hardy *et al.* 1971	pressure vessel	$P \approx 1.14$ GPa
Zha *et al.* 1986	DAC	$P \approx 6.0$ GPa
Theory		
Ross 1973	see ref.	$T \approx 1200$ K, $P \approx 12.78$ GPa
Zha *et al.* 1986	see ref.	$T \approx 3000$ K, $P \approx 53.16$ GPa
Belonoshko 1992	(MD)	$T \approx 4000$ K, $P \approx 92.5$ GPa

experiment argon served as both a medium and a sample, with iron foil as an the absorber of the YAG laser radiation.

Current measurements of iron melting curves diverge significantly beyond the quoted errors above 40 GPa and it is this pressure region that we have examined using a solid argon pressure medium. A 10 μm thick pure iron (99.99%) foil was used as a sample and placed onto an equally thin polished wafer of corundum (figure 2) to provide thermal insulation from the lower diamond surface. The remainder of the sample chamber was filled with argon fluid at 200 MPa. The results presented below were obtained from multiple loadings required to avoid contacting of the sample with the diamond at high pressures.

(*a*) *Melting criteria*

At low pressures near 10 GPa it is possible to observe a clear liquid–solid phase boundary in argon on heating. Figure 2*c*, *d* shows a boundary between melt and solid at roughly constant radius from the foil edge that increases with temperature. At higher pressures, no boundary between fluid and solid can be detected in this way. The scattered coherent light from an Ar^+ laser used to illuminate the sample in the DAC produces a characteristic speckle interference pattern from any metal foil (including the gasket) that is static at fixed temperature (figure 3*b*–*d*). A contribution to the pattern arises from surface texture of the sample, but we also observe changes in the pattern that occur on heating and must be attributable to refractive index contrast or internal reflection at the grain boundaries of argon crystallites. Heating at low laser power, where temperatures are too low to cause detectable emission, we see

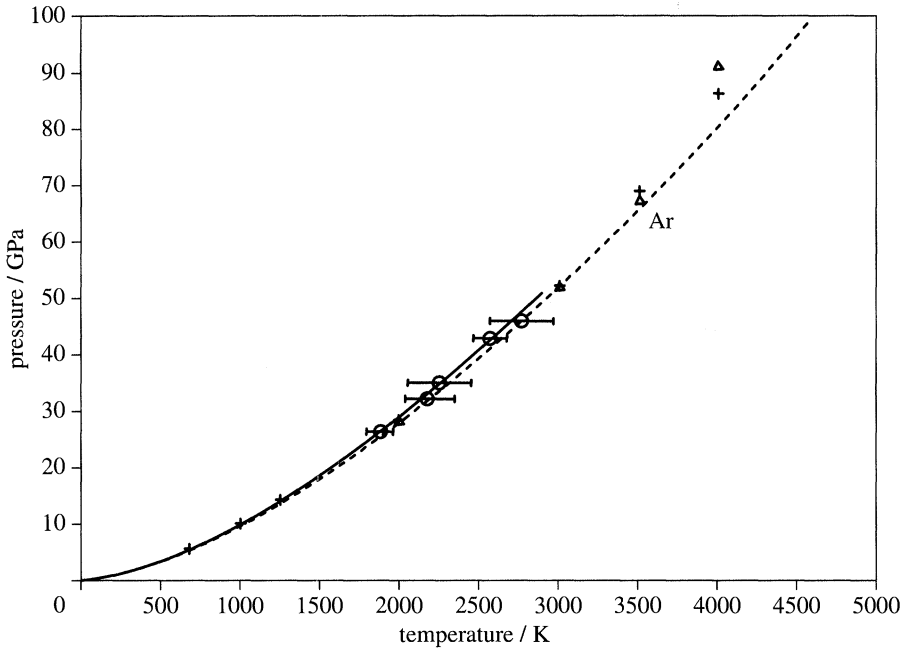

Figure 8. The melting curve of argon. Open circles with temperature error bars are data from this study. Solid line is guide fit to the experimental data. The dashed line is a plot of the SG parametrization of the melting curve determined by Hardy *et al.* (1971) to 1.14 GPa and is negligibly different from the data within the large error on temperature. The open triangles are points from a MD simulation of Belonoshko (1992) to 4000 K, and the crosses the fit of a SG relation to the simulated data. The melting data of Ross (1973) and Zha *et al.* (1986) also agree well with the SG curve determined by Hardy *et al.* (1971). Temperatures were measured from an iron foil absorber.

a discontinuous expansion in the speckle pattern, without apparent breakup of grain boundaries indicating that the pattern is sensitive to thermal expansion of either or both the metal foil and overlying argon. At higher powers, grain boundary motion (or what appears as diffusion and recrystallization) is continuous in time and can, by lowering the laser power, be reduced to a small area coincident with the spatial filtering aperture. Figure 3*c*, *d* shows the small differences in structure that can be detected in the speckle pattern – changes are more easy to detect during continuous observation. The onset of this grain-boundary reconstruction which is interpreted as melting (rather than a pre-melting phenomenon) is well correlated with any irregular shape of the hot parts of the foil due to varying absorption over the extended area that can be heated with a multimode beam. We see a sharp onset with increasing temperature supporting the use of this criterion as a diagnostic of melting in argon. We have observed similar disturbances in the speckle intensity from foils heated in a gas atmosphere which provides further support for the effect being due to refractive index changes arising from density perturbations of the overlying medium. We do not observe annealing of the argon melt to form larger single crystals on reducing the laser power, and this could be because the cooling rate is too high or the aspect ratio of the sample is unfavourable. More precise methods exist for the determination of melting of simple solids in the DAC such as the isochoric change in pressure described by Loubeyre *et al.* (1993), but these methods work effectively because the whole

Table 4. *Melting data for argon*

run	pressure/GPa	temperature/K minimum	temperature/K maximum
Fear7	26.21	1783[a]	1934[a]
Ar7	32.44	2158[a]	2233[a]
Ar15	34.80	2161[a]	2336[a]
Ar8	42.37	2492[a]	2674[a]
Ar16_27,8	47.16	2558[a]	2948[a]
Fa9_600	57.20	2640[b]	—

[a]Melting observed; [b]no melting observed.

sample volume changes phase and would be difficult to apply at the much higher pressures of the present experiments.

The criterion we used for the melting of iron was the appearance of a hole in the foil as we find that melting in argon concealed any texture change in the metal surface under coherent light. In multimode heating, small variations in the temperature of the foil surface are generated, perhaps by change in roughness and absorption, and, near the melting temperature micro-holes appear at random positions. At a pressure of *ca.* 57 GPa we were unable to melt either iron or argon with the laser in CW mode, probably because the gasket became too thin to insulate the sample effectively (the cell as a whole becomes too hot to touch). We make the assumption that temperature gradients into the foil, below the surface, are sufficiently small that no overheating occurs at the surface. This could be tested in future with thinner foils.

(*b*) *Argon melting*

Table 4 lists the melting data on argon we obtained to 47 GPa from the speckle contrast method described above, and plotted in figure 8. The error bars shown in figure 8 correspond to maximum and minimum temperatures measured during a sequence of 100 exposures at constant laser power on the threshold of melting (table 4). The melting curve of argon follows, within error, extrapolation of the SG equation based on data of Hardy *et al.* (1971) to 1.1 GPa at high pressures to at least 47 GPa.

(*c*) *Iron melting*

In figure 9 we plot the existing bounds on the melting line of iron from Williams *et al.* (1987) (Fe (B)), Boehler *et al.* (1990), Boehler (1993), Shen *et al.* (1993) (Fe (M,U)). Figure 9 also shows the superposition of the argon melting curve from our data in figure 8. Depending on choice of the iron melting curve, the argon melting curve should intersect the iron melting curve at pressures near *ca.* 40 GPa or *ca.* 65 GPa.

At 47 GPa iron was observed to melt in various regions of the broad hot spot. In all determinations of Ar melting below 45 GPa with iron as the absorbing material, melting of iron was not observed. As the pressure was raised toward 47 GPa, the argon melting curve and the iron melting curve had become much closer than at

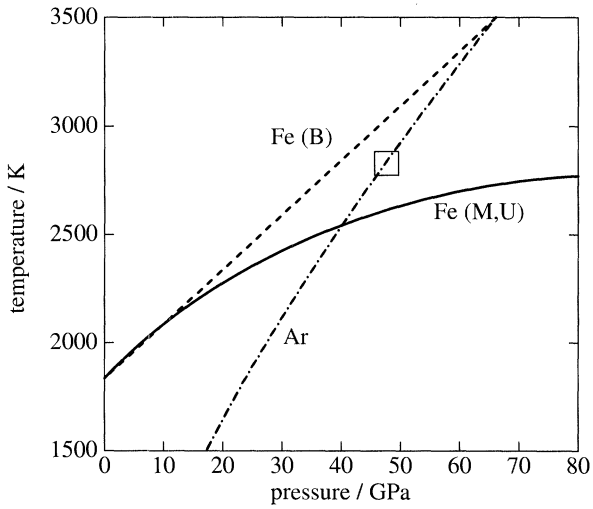

Figure 9. Superposition of the available data on the melting of iron and the melting curve of argon as represented by the Simon equation and the data of this study. Melting lines of iron are sketched from measurements at Berkeley (B) and Mainz and Uppsala (M,U). We observe apparent equality of the melting points of solid argon and iron at 47±1.0 GPa and 2750±300 K (large open square).

Table 5. *Melting data for iron*

run	pressure/GPa	temperature/K minimum	temperature/K maximum
Fe2	20.77	1982[a]	2308[a]
Ar9	28.20	2181[a]	2430[a]
Fe13,14	31.96	2424[a]	2733[a]
Fa9_600	57.20	2640[b]	—

[a]Melting observed; [b]no melting observed.

lower pressure, judged by the simultaneous onset of grain boundary motion and the appearance (at random positions) of microholes in the foil. (As mentioned previously, with multimode laser heating the high-temperature region can be more than ten times larger than the sampling aperture. In addition, the regions of the foil that did melt were not visibly brighter indicating that the temperature was not significantly different to that measured from the sampling aperture.) Table 5 contains the melting temperature of iron we obtain at lower pressures. Our data at low pressure are consistent with previous data and are not plotted in figure 9. On the basis of these observations, equality of the melting points of solid argon and iron at appears to occur at 47±1.0 GPa and 2750±300 K (figure 9). It appears that the Fe (M,U) curve is a lower bound on the iron melting curve, a result further supported by the fact that we were unable to melt iron at 57 GPa in solid argon, despite reaching a temperature of 2640 K (table 5).

6. Discussion

The essential result from the present experiments is that the argon melting curve intersects that of iron near 47 GPa. Several factors could make the pressure of the intersection point uncertain. First, it may be that the melting onset identified with the appearance of argon melt is not correct. This is difficult to envisage because the agreement with both previous experimental work and theoretical calculations would then be coincidental and could be tested with new theoretical techniques. Second, temperatures could be incorrect, either due to measurement inaccuracies or an overshoot of the equilibrium melting point. An important consideration is the effect of thermal gradients and thermal pressure. Because we sample light from the hot spot over a 0.003 mm^2 area, and visual observation suggests that the brightness of the spot is uniform, we assume we are effectively point sampling the temperature profile with no need to correct for temperature gradients. Further, the input power at the sample can be reduced until the point where grain boundary motion is minimal and occupies only the region of the sampling aperture. Pressures were determined before and after heating from ruby fluorescence at room temperature. Because argon is a deformable medium, the role of thermal pressure effects in the region of the hotspot is uncertain: we melt a fraction of the sample volume and further experiments could be made monitoring the pressure continuously away from the heated region. The increase in pressure expected in the area of the laser-heated spot is currently open to question (Heinz 1990).

Boehler *et al.* (1990) reported melting of iron in an argon medium to 35 GPa. At this pressure the argon melting temperature would have been near 2300 K while they reported iron melting at an identical temperature within experimental uncertainty. We found that optical disturbances in argon under coherent illumination on melting make it nearly impossible to detect melting in the two substances simultaneously. No mention of these effects was made by Boehler *et al.* (1990) or in other studies on perovskite, MgO and iron compounds.

Hard, incompressible insulators such as Al_2O_3 appear equally efficient as insulators although chemical reactivity at pressures near 100 GPa could occur (Yoo *et al.* 1995). Our results do not resolve the iron melting curve problem and a comparison of both ionic and molecular thermal insulators may ultimately provide the best confirmation of the iron melting curve and validity of the LHDAC method in general.

That the argon melting curve in this study agrees with data to only 1.1 GPa on the basis of the SG fit is surprising. The SG relation is a single-phase theory that, as discussed above, is equivalent to the Lindemann criterion under special conditions and can be exact if effective pairwise inverse-power repulsive forces dominate (Loubeyre 1989). Over the density range explored along the compression curve solid and fluid must scale identically. Our results are supported by independent theoretical calculations that also agree with the SG relation (Belonoshko 1992; Zha *et al.* 1986; Ross 1969). We see no evidence for a limiting T_m as the pressure is increased. This behaviour is similar to the successful description of the ^{4}He melting curve to 18 GPa with the SG relation fit to data up to 1 GPa.

The relative position of melting points of different materials as a function of pressure offers the potential to constrain temperature independently of its absolute measurement. In particular, a well characterized crossover in melting could be used to compare different experimental methods by providing a fixed point – the coincidence of melting only is important. The accurate characterization of these points may en-

PHILOSOPHICAL TRANSACTIONS OF THE ROYAL SOCIETY A MATHEMATICAL, PHYSICAL & ENGINEERING SCIENCES

able both questions of absolute temperature measurement and melting onset to be addressed in an unbiased way and remove much of the technical uncertainty that can arise in choice of method of obtaining temperature.

This crossing of the melting curves in the P–T plane also occurs in other systems although no attempts have been made to observe the melting points simultaneously. For example, recent single-phase data indicates that wüstite crosses the iron melting curve near 15 GPa and 2200 K, above which pressure the oxide melts at a higher temperature (Shen *et al.* 1993). Similarly, the corundum and stishovite curves intersect near 15 GPa and 3300 K (Shen & Lazor 1995). The recent MgO melting data as noted by Zerr & Boehler (1994) would cross their perovskite melting curve at 50 GPa and 4100 K.

The use of the common melting points of the heavy RGS and metals offers the possibility for a number of crossover standard fixed points in the P–T plane to be defined, provided chemical interaction between solid and RGS does not occur. It remains to be seen whether the heavier, more polarizable, RGS melt at temperatures that obey the SG relation predictions from lower-pressure melting data; for example, solid xenon could melt near 4000 K at 20 GPa. Early measurements on solid Kr and Xe do in fact suggest that the heavy RGS melt at comparatively high temperatures for a given pressure (Jephcoat & Besedin 1996, in preparation). The heavy RGS melting curves, in combination with selected metals, could then be used to map a wide region of the P–T plane.

This work was supported by the Royal Society (London) and the UK NERC Grant numbers GR3/07673A and GR9/01570. S.P.B. acknowledges the Royal Society for support under an FSU Research Fellowship.

References

Al'tshuler, L. V., Bakanova, A. A. & Trunin, R. F. 1962 Shock adiabats and zero isotherms of seven metals at high pressures. *Sov. Phys. JETP* **15**, 65–74.

Anderson, O. L. 1990 The high-pressure triple points of iron and their effects on the heat flow from the Earth's core. *J. Geophys. Res.* **95**, 21697–21707.

Anderson, O. L. 1995 Mineral physics of iron and of the core. *Rev. Geophys.* **33**, 429–441.

Anderson, O. L. & Duba, A. G. 1996 The experimental phase diagram of iron revisited. *Geophys. Jl Int.* (Submitted.)

Bass, J. D., Svendsen, B. & Ahrens, T. J. 1987 The temperature of shock compressed iron. In *High-pressure research in mineral physics* (ed. M. H. Manghnani & Y. Syono), pp. 393–402. Tokyo: Terra Scientific; Washington, DC: American Geophysical Union.

Bassett, W. A. & Weathers, M. S. 1987 Temperature Measurements in a laser-heated diamond-anvil cell. In *High-pressure research in mineral physics* (ed. M. H. Manghnani & Y. Syono), pp. 129–133. Tokyo: Terra Scientific; Washington, DC: American Geophysical Union.

Belonoshko, A. B. 1992 Equation of state and melting transition of argon up to 8000 K and 4 Megabars: a molecular dynamics study. *High Pressure Res.* **10**, 583–597.

Belonoshko, A. B. 1994 Molecular dynamics of $MgSiO_3$ perovskite at high pressures: equation of state, structure, and melting transition. *Geochim. Cosmochim. Acta* **58**, 4039–4047.

Birch, F. 1972 The melting relations of iron, and temperatures in the Earth's core. *J. Geophys. Res.* **29**, 373–387.

Bodea, S. & Jeanloz, R. 1989 Model calculations of the temperature distribution in the laser-heated diamond cell. *J. Appl. Phys.* **65**, 4688–4692.

Boehler, R. 1986 The phase diagram of iron to 430 kbar. *Geophys. Res. Lett.* **13**, 1153–1156.

Boehler, R. 1992 Melting of the Fe–FeO and the Fe–FeS systems at high pressure: constraints on core temperatures. *Earth Planet. Sci. Lett.* **111**, 217–227.

Boehler, R. 1993 Temperatures in the Earth's core from melting-point measurements of iron at high static pressures. *Nature* **363**, 534–536.

PHILOSOPHICAL TRANSACTIONS OF THE ROYAL SOCIETY A MATHEMATICAL, PHYSICAL & ENGINEERING SCIENCES

Boehler, R. 1996 Experimental constraints on melting conditions relevant to core formation. *Geochim. Cosmochim. Acta* **60**, 1109–1112.

Boehler, R. & Chopelas, A. 1991 A new approach to laser heating in high pressure mineral physics. *Geophys. Res. Lett.* **18**, 1147–1150.

Boehler, R. & Chopelas, A. 1992 Phase transitions in a 500 kbar–3000 K gas apparatus. In *High-pressure research: application to Earth and planetary sciences* (ed. Y. Syono & M. H. Manghnani), pp. 55–60. Washington, DC: American Geophysical Union.

Boehler, R. & Zerr, A. 1994 High-pressure melting of (Mg,Fe)SiO_3–perovskite. *Science* **264**, 280–281; correction **265**, 723.

Boehler, R., von Bargen, N. & Chopelas, A. 1990 Melting, thermal expansion and phase transitions of iron at high pressures. *J. Geophys. Res.* **95**, 21731–21736.

Boyd, R. W. 1983 *Radiometry and the detection of optical radiation.* New York: John Wiley.

Bridgman, P. W. 1934 The melting parameters of nitrogen and argon under pressure, and the nature of the melting curve. *Phys. Rev.* **46**, 930–933.

Brown, J. M. 1993 Mantle melting at high pressure. *Science* **262**, 529–530.

Brown, J. M. & McQueen, R. G. 1986 Phase transitions, Grüneisen parameter, and elasticity for shocked iron between 77 GPa and 400 GPa. *J. Geophys. Res.* **91**, 7485–7494.

Brown, J. M. & McQueen, R. G. 1980 Melting of iron under core conditions. *Geophys. Res. Lett.* **7**, 533–536.

Brown, J. M. & McQueen, R. G. 1982 The equation of state for iron and the Earth's core. In *High-pressure research in geophysics* (ed. S. Akimoto & M. H. Manghnani), vol. 12, pp. 611–623. Tokyo: Center for Academic Publications.

Cabannes, F. 1967 Facteurs de réflexion et d'émission des metaux. *J. Phys.* **28**, 235–248.

Cohen, R. & Weitz, J. 1996 The melting curve and premelting of MgO. (In preparation.)

Crawford, R. K. & Daniels, W. B. 1968 Melting in argon at high temperatures. *Phys. Rev. Lett.* **21**, 367–369.

de Vos, J. C. 1954 A new determination of the emissivity of tungsten ribbon. *Physica* **20**, 690–714.

Duba, A. G. 1992 Earth's core not so hot *Nature* **359**, 197–198.

Duba, A. G. 1994 Iron – what is melt? In *High-pressure science and technology – 1993* (ed. S. C. Schmidt, J. W. Shaner, G. A. Samara & M. Ross), pp. 923–926. New York: AIP Press.

Gillet, P., Fiquet, G., Daniel, I. & Reynard, B. 1993 Raman spectroscopy at mantle pressure and temperature conditions Experimental set-up and the example of $CaTiO_3$ perovskite *Geophys. Res. Lett.* **20**, 1931–1934.

Hardy, W. H., Crawford, R. K. & Daniels, W. B. 1971 Experimental determination of the *P*–*T* melting curve of argon. *J. Chem. Phys.* **54**, 1005–1010.

Heinz, D. L. 1990 Thermal pressure in the laser-heated diamond-anvil cell. *Geophys. Res. Lett.* **17**, 1161–1164

Heinz, D. L. & Jeanloz, R. 1987*a* Measurement of the melting curve of (Mg,Fe)SiO_3 at lower mantle conditions and its geophysical implications. *J. Geophys. Res.* **92**, 11437–11444.

Heinz, D. L. & Jeanloz, R. 1987*b* Temperature measurements in the laser-heated diamond cell. *High-pressure research in mineral physics* (ed. M. H. Manghnani & Y. Syono), pp. 113–127. Tokyo: Terra Scientific; Washington, DC: American Geophysical Union.

Heinz, D. L., Sweeney, J. S. & Miller, P. 1991 A laser heating system that stabilizes and controls the temperature: diamond anvil cell applications. *Rev. Sci. Instrum.* **62**, 1568–1575.

Heinz, D. L., Knittle, E., Sweeney, J. S., Williams, Q. & Jeanloz, R. 1994 High-pressure melting of (Mg,Fe)SiO_3–perovskite. *Science* **264**, 279–280.

Jeanloz, R. & Heinz, D. L. 1984 Experiments at high temperature and pressure: laser heating through the diamond cell. *J. Physique (Paris)* **45**(C8), 83–92.

Kennedy, G. C. & Vaidya, S. N. 1970 The effect of pressure on the melting temperature of solids. *J. Geophys. Res.* **75**, 1019–1022.

Knittle, E. & Jeanloz, R. 1989 Melting curve of (Mg,Fe)SiO_3–perovskite to 96 GPa: evidence for a structural transition in lower mantle melts. *Geophys. Res. Lett.* **16**, 421–424.

PHILOSOPHICAL TRANSACTIONS OF THE ROYAL SOCIETY A MATHEMATICAL, PHYSICAL & ENGINEERING SCIENCES

Knittle, E. & Jeanloz, R. 1991 The high-pressure phase diagram of $Fe_{0.94}O$: a possible constituent of the Earth's core. *J. Geophys. Res.* **96**, 16169–16180.

Kormer, S. B. 1968 Optical study of the characteristics of shock-compressed dielectrics. *Sov. Phys. Usp.* **11** 229–254.

Kormer, S. B., Sinitsyn, M. V., Kirilov, G. A. & Urlin, V. D. 1965 Experimental determination of temperature in shock-compressed NaCl and KCl and of their melting curves at pressures up to 700 kbar. *Sov. Phys. JETP* **21**, 689–700.

Lahr, P. H. & Eversole, W. G. 1962 Compression isotherms of argon, krypton and xenon through the freezing zone. *J. Chem. Eng. Data* **7**, 42–47.

Lazor, P., Shen, G. & Saxena, S. K. 1993 Laser-heated diamond anvil cell experiments at high pressure – melting curve of nickel up to 700 kbar. *Phys. Chem. Miner.* **20**, 86–90.

Liu, L.-G., Bassett, W. A. 1975 The melting of iron up to 200 kbar. *J. Geophys. Res.* **80**, 3777–3782.

Loubeyre, P., LeToullec, R. & Pinceaux, J.-P. 1993 Experimental investigation of solidification in ^{4}He, ^{3}He, and Ne at very high pressure. *Phys. Rev. Lett.* **70**, 2106–2109.

Loubeyre, P. 1989 Melting at high density. In *Simple molecular systems at very high density* (ed. A. Polian, P. Loubeyre & N. Boccara), pp. 181–201 (NATO ASI Series B: Physics, vol. 186). New York: Plenum

Mao, H.-K., Bell, P. M. & Hadidiacos, C. 1987 Experimental phase relations of iron to 360 kbar, 1400 °C, determined in an internally heated diamond-anvil apparatus. *High-pressure research in mineral physics* (ed. M. H. Manghnani & Y. Syono), pp. 135–138. Tokyo: Terra Scientific; Washington, DC: American Geophysical Union.

McQueen, R. G., Marsh, S. P., Taylor, J. W., Fritz, J. N. & Carter, W. J. 1970 The equation of state of solids from shock-wave studies. In *High velocity impact phenomena* (ed. R. Kinslow), pp. 293–417. New York: Academic Press.

Michels, A. & Prins, C. 1962 The melting lines of argon, krypton and xenon up to 1500 atm; representation of the results by a law of corresponding states. *Physica* **28**, 101–116.

Ming, L.-C. & Bassett, W. A. 1974 Laser heating in the diamond-anvil press up to 2000 °C sustained and 3000 °C pulsed at pressures up to 260 kilobars. *Rev. Sci. Instrum.* **45**, 1115–1118.

Nellis, W. J. & Yoo, C. S. 1990 Issues concerning shock temperature measurements of iron and other metals. *J. Geophys. Res.* **95**, 21749–21752.

Nicholas, J. V. & White, D. R. 1994 *Traceable temperatures.* New York: John Wiley.

Ohtani, E. 1993 Melting temperature distribution and fractionation in the lower mantle. *Phys. Earth Planet Int.* **33**, 12–25.

Poirier, J.-P. 1989 Lindemann law and the melting temperature of perovskites. *Phys. Earth. Planet Int.* **54**, 364–369.

Poirier, J.-P. 1994 Light elements in the Earth's outer core: a critical review. *Phys. Earth. Planet Int.* **85**, 319–337

Quinn, T. J. 1990 *Temperature*, 2nd edn. London: Academic Press.

Robinson, D. W. 1954 An experimental determination of the melting curves of argon and nitrogen into the 10 000 atm region. *Proc. R. Soc. Lond.* **A225**, 393–405.

Ross, M. 1969 Generalized Lindemann melting law. *Phys. Rev.* B **184**, 233–242.

Ross, M. 1973 Shock compression and the melting curve for argon. *Phys. Rev.* A **8**, 1466–1474.

Saxena, S. K., Shen, G. & Lazor, P. 1993 Experimental evidence for a new iron phase and implications for Earth's core. *Science* **260**, 1312–1314.

Saxena, S. K., Shen, G. & Lazor, P. 1994 Temperatures in Earth's core based on melting and phase transformation experiments on iron. *Science* **264**, 405–407.

Saxena, S. K., Dubrovinsky, L. S., Häggkvist, P., Cerenius, Y., Shen, G. & Mao, H.-K. 1995 Synchrotron X-ray study of iron at high-pressure and temperature. *Science* **269**, 1703–1704.

Schmitt, D. & Ahrens, T. J. 1984 Emission spectra of shock compressed solids. In *Shock waves in condensed matter, 1983* (ed. J. R. Asay, R. A. Graham & G. K. Straub), pp. 313–316. New York: Elsevier.

PHILOSOPHICAL TRANSACTIONS OF THE ROYAL SOCIETY A MATHEMATICAL, PHYSICAL & ENGINEERING SCIENCES

Schneider, W. E. & Goebel, D. G. 1984 Standards for calibration of optical radiation measurement systems. *Laser Focus Electro-Optics* **20**, 82–90.

Shen, G. Y. & Lazor, P. 1995 Measurement of melting temperatures of some minerals under lower mantle pressures. *J. Geophys. Res.* **100**, 17 699–17 713.

Shen, G. Y., Lazor, P. & Saxena, S. K. 1993 Melting of wüstite and iron up to pressures of 600 kbar. *Phys. Chem. Miner.* **20**, 91–96.

Shen, G. Y., Mao, H.-K., Hemley, R. J. 1996 Laser-heated diamond anvil cell technique: double-sided heating with multimode Nd:YAG laser. In *Proc. 3rd NIRIM Int. Symp. on Advanced Materials*, pp. 149–152. Tokyo: International Communication Specialists.

Simon, F., Ruhemann, M. & Edwards, W. A. M. 1930 *Z. Phys. Chem.* B **6**, 62.

Simon, F. E. 1953 The melting of iron at high pressures. *Nature* **172**, 746–747.

Stishov, S. M., Makarenko, I. N., Ivanov, V. A. & Fedosimov, I. V. 1970 Melting of argon at high temperatures. *Zh. Eksp. Teor. Fiz. Pis'ma Red.* **11**, 22. (*JETP Lett.* **11**, 13–15.)

Stishov, S. M. 1975 The thermodynamics of melting of simple substances. *Sov. Phys. Usp.* **17**, 625–643.

Stixrude, L. & Bukowinski, M. S. T. 1990 Fundamental thermodynamic relations and silicate melting with implications for the constitution of D″. *J. Geophys. Res.* **95**, 19 311–19 325.

Strong, H. M., Tuft, R. E. & Hannemann, R. E. 1973 The iron fusion curve and the triple point. *Metall. Trans.* **4**, 2657–2611.

Svendsen, B., Bass, J. D. & Ahrens, T. J. 1989 Optical radiation from shock-compressed materials and interfaces *Phys. Rep. (Phys. Lett.)* **180**, 333–416.

Sweeney, J. S. & Heinz, D. L. 1993*a* Melting of iron–magnesium–silicate perovskite. *Geophys. Res. Lett.* **20**, 855–858.

Sweeney, J. S. & Heinz, D. L. 1993*b* Thermal analysis in the laser-heated diamond anvil cell. *Pure Appl. Geophys.* **141**, 497–507.

Taylor, J. E. 1952 The variation with wavelength of the spectral emissivity of iron and molybdenum. *J. Opt. Soc. Am.* **42**, 33–36.

Touloukian, Y. S. & DeWitt, D. P. 1970 *Thermal radiative properties of metallic elements and alloys*. New York: IFI/Plenum.

Vočadlo, L. & Price, G. D. 1996 The melting of MgO – computer calculations via molecular-dynamics. *Phys. Chem. Miner.* **23**, 42–49.

Williams, Q. & Jeanloz, R. 1990 Melting relations in the iron–sulphur system at ultrahigh pressures: implications for the thermal state of the Earth. *J. Geophys. Res.* **95**, 19 299–19 310.

Williams, Q., Jeanloz, R., Bass, J., Svendsen, B. & Ahrens, T. J. 1987 The melting curve of iron to 250 gigapascals: a constraint on the temperature at Earth's centre. *Science* **236**, 181–182.

Williams, Q., Knittle, E. & Jeanloz, R. 1991 The high-pressure melting curve of iron: a technical discussion. *J. Geophys. Res.* **96**, 2171–2184.

Yagi, T. & Susaki, J. 1992 A laser heating system for the diamond-anvil cell using CO_2 laser. *High-pressure research: application to Earth and planetary sciences* (ed. Y. Syono & M. H. Manghnani), pp. 51–54. Washington, DC: American Geophysical Union.

Yoo, C. S., Holmes, N. C., Ross, M., Webb, D. J. & Pike, C. 1993*a* Shock temperatures and melting of iron at Earth core conditions. *Phys. Rev. Lett.* **70**, 3931–3934.

Yoo, C. S., Akella, J. & Moriarty, J. A. 1993*b* High-pressure melting temperatures of uranium: laser-heating experiments and theoretical calculations. *Phys. Rev.* B **48**, 15 529–15 534.

Yoo, C.-S., Akella, J., Campbell, A. J., Mao, H.-K. & Hemley, R. J. 1995 Phase-diagram of iron by *in situ* X-ray diffraction – implications for Earth's core. *Science* **270**, 1473–1475.

Zerr, A. & Boehler, R. 1993 Melting of (Mg,Fe)SiO_3–perovskite to 625 kilobars: indication of a high melting temperature in the lower mantle. *Science* **262**, 553–555.

Zerr, A. & Boehler, R. 1994 Constraints on the melting temperature of the lower mantle from high-pressure experiments on MgO and magnesiowüstite. *Nature* **371**, 506–508.

Zha, C.-S., Boehler, R., Young, D. A. & Ross, M. 1986 The argon melting curve to very high pressures. *J. Chem. Phys.* **85**, 1034–1036.

PHILOSOPHICAL TRANSACTIONS OF THE ROYAL SOCIETY A MATHEMATICAL, PHYSICAL & ENGINEERING SCIENCES

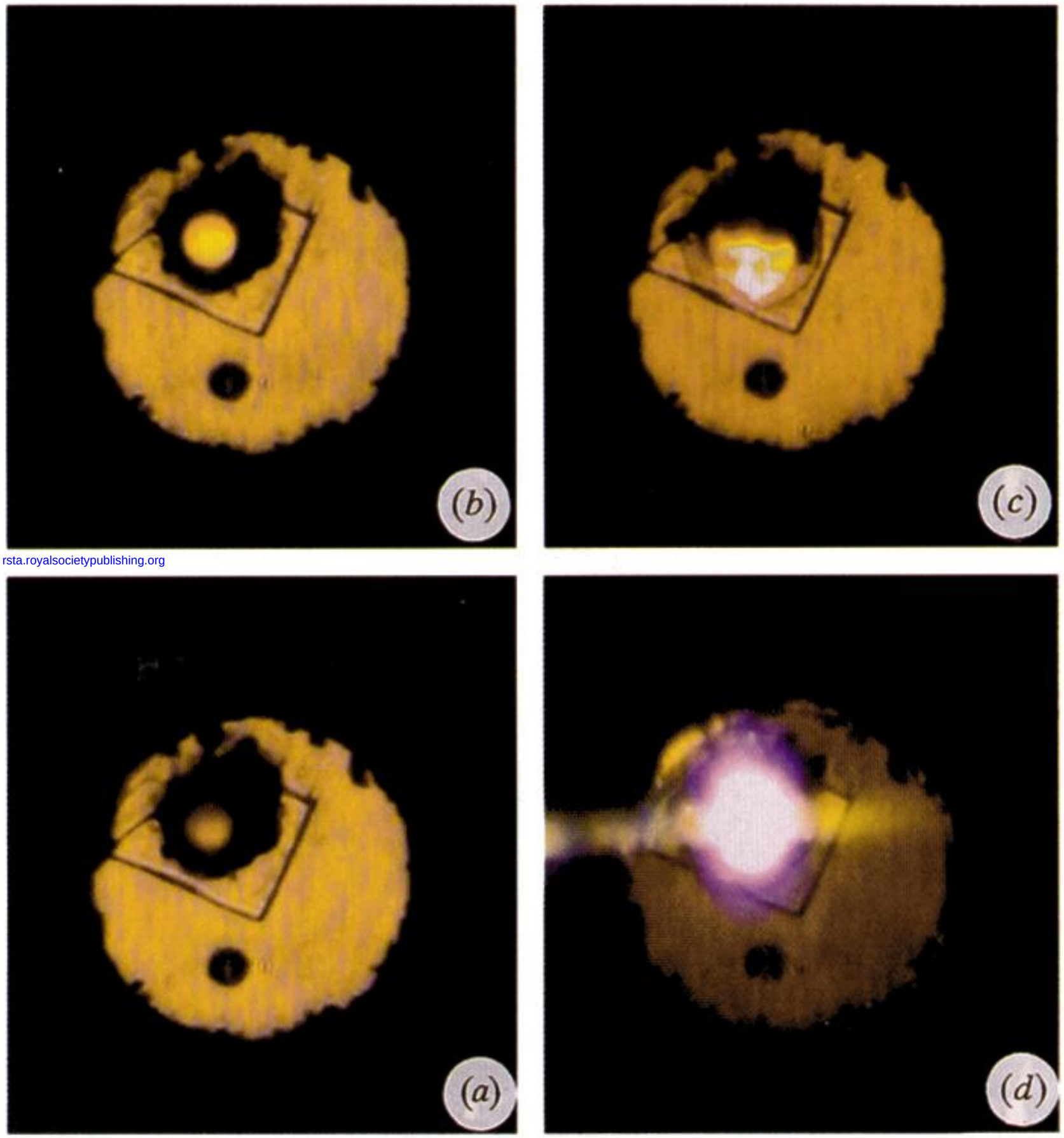

igure 2. Demonstration of laser-heated spot in the DAC generated with a TEM_{00} mode YAG ser beam focused on iron foil in solid argon at 10 GPa. The foil is resting on a Al_2O_3 wafer insulate it from the lower diamond within a 0.15 mm hole drilled into a stainless-steel gas- et. Transmitted light provides general background illumination through the transparent, solid rgon. The panels (*a*)–(*d*) show a progressive increase in intensity of the laser and the axially mmetric focus that can be formed with this mode. Saturation of the video camera used to apture the image takes place in (*d*) as the temperature rises. Temperatures would be measured collecting light from an area of roughly one fifth the diameter of the hot spot (0.015 mm). A elt boundary between fluid and solid argon is observed in (*c*) and (*d*) as indicated by a dark ne roughly following the outline of the heated foil.

PHILOSOPHICAL TRANSACTIONS OF THE ROYAL SOCIETY A MATHEMATICAL, PHYSICAL & ENGINEERING SCIENCES

igure 3. Demonstration of the speckle interference pattern observed through a narrow-pass lter with a sample illuminated with blue 488 nm light of an Ar^+ laser. The size of the hotspot *ca.* 0.015 mm. (*a*) shows hot spot in transmitted light without laser illumination and filter and) the speckle pattern generated under coherent light. The circled regions in (*c*) and (*d*) show ıe slight change in the speckle pattern as observed through the filter and used to determine ıe melting in solid argon in this study.